AIP Journal of Applied Physics

Enhanced piezoelectric performance from carbon fluoropolymer nanocomposites

Cary Baur, Jeffrey R. DiMaio, Elliot McAllister, Reza Hossini, Earl Wagener, John Ballato, Shashank Priya, Arthur Ballato, and Dennis W. Smith Jr.

Citation: Journal of Applied Physics **112**, 124104 (2012); doi: 10.1063/1.4768923
View online: http://dx.doi.org/10.1063/1.4768923
View Table of Contents: http://scitation.aip.org/content/aip/journal/jap/112/12?ver=pdfcov
Published by the AIP Publishing

Enhanced piezoelectric performance from carbon fluoropolymer nanocomposites

Cary Baur,[1,3] Jeffrey R. DiMaio,[2,3] Elliot McAllister,[3] Reza Hossini,[2] Earl Wagener,[2,3] John Ballato,[4] Shashank Priya,[3] Arthur Ballato,[5] and Dennis W. Smith, Jr.[1,3,a)]
[1]*Department of Chemistry, and The Alan G. MacDiarmid Nanotech Institute, The University of Texas at Dallas, 800 W. Campbell Road, Richardson, Texas 75080, USA*
[2]*Tetramer Technologies L.L.C., 657 S. Mechanic Street, Pendleton, South Carolina 29670, USA*
[3]*Center for Energy Harvesting Materials and Systems (CEHMS), Virginia Polytechnic Institute and State University, Blacksburg, Virginia 24061, USA*
[4]*Department of Material Science and Engineering and the Center for Optical Materials Science and Engineering Technologies (COMSET), Clemson University, Clemson, South Carolina 29634, USA*
[5]*Holcombe Electrical and Computer Engineering, Clemson University, Clemson, South Carolina 29634, USA*

(Received 15 October 2012; accepted 10 November 2012; published online 17 December 2012)

The piezoelectric performance of polyvinylidene fluoride (PVDF) is shown to double through the controlled incorporation of carbon nanomaterial. Specifically, PVDF composites containing carbon fullerenes (C_{60}) and single-walled carbon nanotubes (SWNT) are fabricated over a range of compositions and optimized for their Young's modulus, dielectric constant, and d_{31} piezoelectric coefficient. Thermally stimulated current measurements show a large increase in internal charge and polarization in the composites over pure PVDF. The electromechanical coupling coefficients (k_{31}) at optimal loading levels are found to be 1.84 and 2 times greater than pure PVDF for the PVDF-C_{60} and PVDF-SWNT composites, respectively. Such property-enhanced nanocomposites could have significant benefit to electromechanical systems employed for structural sensing, energy scavenging, sonar, and biomedical imaging. © *2012 American Institute of Physics*.
[http://dx.doi.org/10.1063/1.4768923]

I. INTRODUCTION

A piezoelectric material converts mechanical stress to electrical charge, referred to as the "direct" effect, and converts an electric field to mechanical strain, the "converse" effect.[1,2] Piezoelectric materials belong to non-centrosymmetric point groups which result in net distortion from the equilibrium position with the application of stress or an electric field.[3] The direct piezoelectric effect is classically utilized in structural measurement, pressure sensors, and vibrational energy-scavenging, while the converse piezoelectric effect is useful for active vibrational dampening, shape control, and actuation.[4–7]

The first piezoelectric material to be used practically and at a large scale was single-crystal quartz (SiO_2) because of its piezoelectric nature and low acoustic loss. While quartz offers high quality factors, polycrystalline ceramics based on lead zirconium titanate (PZT) or barium titanate also exhibit large piezoelectric coefficients with high electromechanical coupling. These materials, however, are naturally limited by their requisite large driving voltages, high stiffness, brittleness, and low processability. For many growing, high-value applications, compliant materials with lower mechanical impedance, cost, and driving voltages are required.[8]

The discovery of piezoelectricity in semicrystalline polyvinylidene fluoride (PVDF) by Kawai in 1969 introduced a new highly flexible and processable material.[9] The alternating repeat unit (CH_2-CF_2) allows for two dominant crystalline phases, referred to as α and β. As shown in Figure 1, the α phase arranges in a centrosymmetric unit cell, resulting in a nonpolar crystal, while the β phase is an all trans planar zigzag conformation that results in a polar, noncentrosymmetric crystal with a large dipole when electrically poled.[10]

The discovery of piezoelectric polymers offers a relatively new class of elastically compliant, low dielectric materials, referred to as electroactive polymers (EAPs).[12–14] EAPs have been incorporated into a broad range of applications such as actuators, integrated microelectromechanical systems, sensors, ultrasonic imaging, and ferroelectric memory devices.[15] However, low voltage and force generation capabilities have greatly limited their application.[16]

Newnham *et al*. introduced an electroactive composite which combined a passive polymer matrix with piezoelectric ceramic particles in order to utilize the distinct advantages of each material.[17–19] More recently, carbon nanotubes (CNTs) have been used to improve piezoelectric performance of EAPs through an increase in Young's modulus.[20–22] However, no comprehensive mechanism of piezoelectric enhancement has been reported. Buckminster fullerenes (C_{60}) are comprised of an sp^2 hybridized structure similar to that of CNTs, but are spherical as opposed to the tubular structure of CNTs.[23] The difference in size and geometry (shown in Figure 1) of these particles, while similar in structure and electrical properties, allows for a useful comparison to be made, and mechanisms of enhancement to be illuminated.

a)Author to whom correspondence should be addressed. Electronic mail: dwsmith@utdallas.edu.

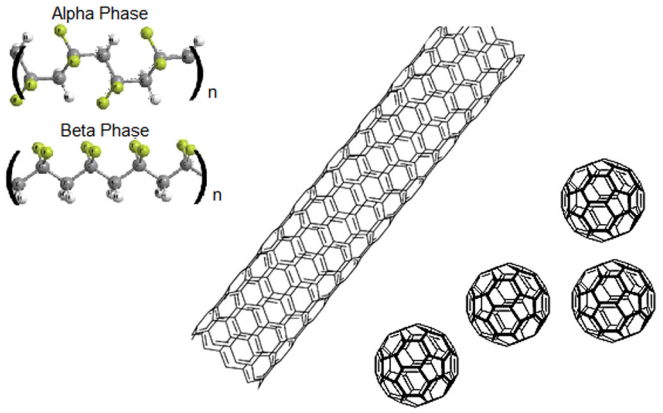

FIG. 1. Structure of α and β phase PVDF (top left)[11] Representations of C_{60} (bottom right) and SWNT (middle).

In this work, nanocomposites of single-walled carbon nanotubes (SWNTs) and fullerenes (C_{60}) with PVDF are reported including previously unexplored characterization and enhancement mechanisms. The analysis provided herein not only focuses on the piezoelectric enhancement due to improvements in mechanical properties but also explores the changes in morphology, relative dielectric constant (ε_r), charge storage, and charge release of the material. For the first time, a more complete picture of the mechanisms of piezoelectric enhancement in nanocomposites is explored. Through the introduction of charge and by altering Young's modulus (Y) and relative dielectric constant (ε_r), a maximum value of above 60 pC/N is achieved for both the C_{60} and SWNT nanocomposites, twice the performance of pure PVDF.

II. METHODS

PVDF (weight average molecular weight Mw, of 180 000 $gmol^{-1}$, number average molecular weight, Mn, of 71 000 $gmol^{-1}$) and dimethylacetamide (DMAC) were obtained from Sigma Aldrich. C_{60} (99.5% pure) and SWNTs (97% pure) were purchased from Nano-C, Inc., (*Westwood, MA)* and used as received.

A. Sample fabrication

The nanoparticles were dispersed in DMAC by ultrasonication (Vertis 115 V sonicator) in a beaker for an hour with the gradual addition of PVDF granules to avoid aggregation. PVDF was then dissolved at 20 wt. % in the solution to create a stock solution. The solution then was cooled and solvent was removed through dropwise addition into circulating deionized water. The resultant solids were dried at 90 °C under vacuum for 24 h and then extruded using a twin screw melt extruder with a 25.4 mm die. Commercial stretched and poled PVDF films (40 μm thick) were purchased from Piezotech (Hésingue, France).

B. Drawing and poling

Samples were drawn using an in-house variable speed stretching system, and were drawn to 4 times their original length in a heated silicon oil bath at 80 °C to ensure a consistent temperature throughout the material. Samples were 50 μm in thickness and 13 mm wide after drawing, and were cleaned and electroded with copper using a Ladd vapor deposition system prior to poling at 20 kV and 80 °C for 20 min in a high dielectric breakdown liquid (Fluorinert from 3M). The samples then were quenched to room temperature while remaining under the applied voltage.

C. Material testing

A Mettler-Toledo differential scanning calorimeter (DSC) was used to observe thermal behavior of samples from 0 °C to 220 °C with a heating rate of 1 °C/min and cooling rate of 5 °C/min. Transmission electron microscopy images were obtained using a (TEM)-Hitachi H7600T transmission electron microscope at 110 kV. Thermally stimulated current measurements were conducted with a Solomat thermally stimulated current relaxation mapping analysis spectrometer (TSC/RMA). 1 by 1 cm wide (50 μm thick) stretched and electroded samples were polarized by applying a DC field of 1×10^4 Vcm^{-1} for 5 min at 75 °C followed by a rapid cooling to −75 °C with the field still applied. The field was then removed and samples were heated at a rate of 5 °C/min to 160 °C. The Young's modulus was found using an Instron 5582 following the ASTM D638-10 standard, taking an average of five measurements per reported value with the standard deviation under ±5%. Hysteresis curves were obtained using a Radiant Technologies Precision Premier ferroelectric testing device based on the modified Sawyer Tower technique. A voltage from −10 to 10 V was swept continuously on the samples at a frequency of 1 Hz. Conductivity measurements were conducted with a four-point probe.

D. Piezoelectric testing

The direct piezoelectric coefficient is defined as the reversible change in polarization of a material when it experiences a change in applied stress. In practice, however, this effect is determined from the charge Q induced on a sample of cross-sectional area A undergoing a change in stress.[24] A quasi-static experimental setup (Figure 2) was used for piezoelectric measurements in which samples were fixed from the top and a 47 g mass was suspended from the bottom, pulling the sample along its length.[12] A force of 0.46 N was applied with a constant period of 10 ms. Leads were attached to the surface electrodes, and connected to a Rigol oscilloscope to monitor the resulting voltage, with a capacitor in parallel. The capacitance of the samples was very low, thus the charge that accumulated on the sample electrodes during loading and unloading was almost entirely transferred to the capacitor, with the resulting voltage being measured by the oscilloscope. Five samples of each wt. % were tested and standard deviations of all samples were under ±5%.

The applied force and the resulting charge were used to determine the material's d_{31} piezoelectric strain constant using the below equation

$$d_{31} = \frac{Q_3}{F_1}. \quad (1)$$

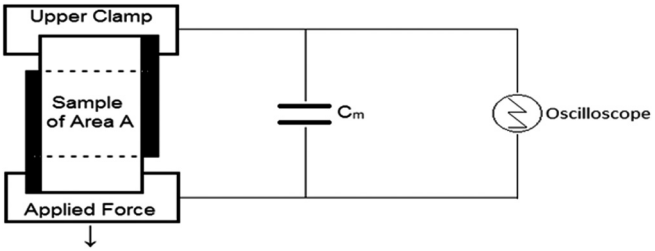

FIG. 2. Schematic of piezoelectric testing setup.

III. RESULTS AND DISCUSSION

A. Material testing

Nanocomposites were solution mixed and melt extruded into films (see experimental) at variable weight percentages of the nanoparticles (0–0.25 wt. %) relative to the PVDF content. There was no apparent reaction between the particles and host during synthesis, stretching, or poling. The differential scanning calorimetry thermograph shown in Figure 3(a) allowed for the determination of the melting behavior of the composites. Pure PVDF shows a two-phase melting peak, with a dominant melt at 166 °C and a weaker melt at 170 °C. This is due to a bimorphic structure within the crystalline regions of the material. When C_{60} is added at 0.1 wt. % to the PVDF only one visible melting peak is observed, with a very small, higher melting temperature shoulder. The addition of SWNTs at 0.1 wt. % results in a monomorphic material with only one apparent melt transition. The appearance of one phase in the material suggests that the nanoparticles are acting as nucleation sites, allowing for simultaneous growth of crystallites, resulting in a smaller crystallite size and greater uniformity as discussed next.

Transmission electron microscopy, Figure 3, shows a very clear stacked lamella structure with a fibrous appearance in pure PVDF (b). However, a small, uniform lamella structure generally oriented in line with the nanotubes is seen in the SWNT composite (c). These images suggest that smaller, more uniform crystallites are being nucleated through the addition of nanoparticles. These data support an expected enhancement to the piezoelectric effect as a more uniform material containing smaller crystallites is advantageous for facilitation of charge storage through the addition of interfaces.[25] Interfacial dynamics are well-known to play an important part in contributing toward the electromechanical response.

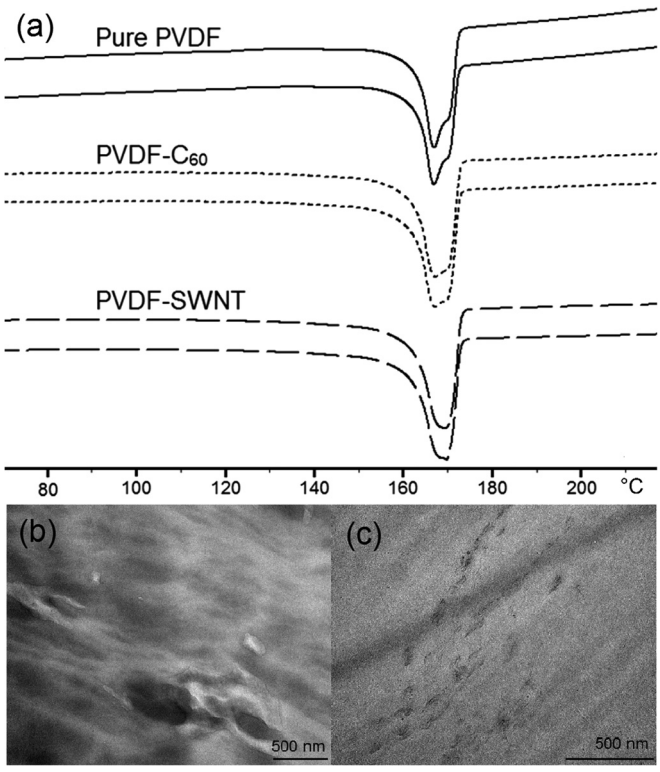

FIG. 3. (a) DSC curves of PVDF, PVDF-C_{60} (0.1 wt. %) and PVDF-SWNT (0.1 wt. %) (b) TEM image of pure PVDF (c) TEM image of PVDF-SWNT (0.1 wt. %).

B. Internal charge testing

Figure 4 shows the TSC spectra of the C_{60} and SWNT PVDF nanocomposites at 0.1 wt. % relative to pure PVDF. The amount of current generated by the nanocomposites was much greater than that for pure PVDF; therefore, the spectra are normalized to pure PVDF.

TSC has been widely used in the past for the detection of trapped charges in polymers.[26] Upon heating of a charge-storing material, transient charges are released, and can be characterized, according to the temperature dependence of current generation. For example, charges can be injected into macroscopic voids in porous polymers to create oriented, "quasi-dipoles", known as electrets.[26] Through TSC, it has been shown that internal charge of a porous polymer can be increased by 50 times through the creation of space charge through charge injection.[27] Likewise, charge also can be trapped at dielectric boundaries such as adjoining crystalline/amorphous regions, called interfacial polarization.[28] Segmental mobility of interfacial charges increases upon heating to allow "hopping" between charged surface reservoirs to create current bands.[29] The deeper and more isolated the charge, the higher the release temperature, generally. The concept of developing interfacial charge has been well

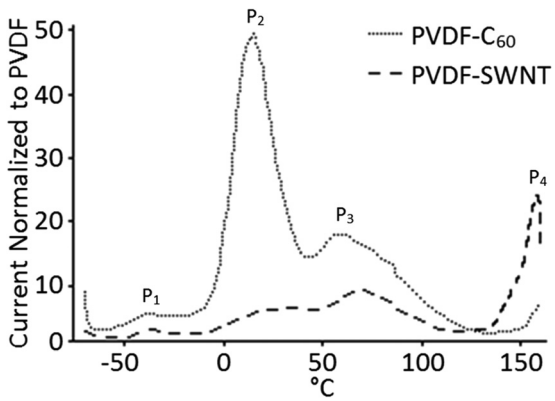

FIG. 4. TSC spectra of differential current produced from 0.1 wt. % PVDF-SWNT and PVDF-C_{60} normalized to PVDF.

explored, and TSC spectra of charge containing PVDF have been reported.[30]

Known from past literature is that there are four dominant peaks in a TSC curve of poled PVDF; two corresponding to the relaxation of polarized dipoles and two due to trapped charge in the material.[31] The spectral peaks measured here agree with the literature, clearly showing four dominant peaks, however the current discharged is much greater than those reported for pure PVDF.

The first peak, P_1, can be attributed to the depolarization of dipoles due to relaxation of the amorphous phase at the glass transition. At this temperature, relaxation begins to occur due to micro-Brownian motion in the amorphous main chain, allowing aligned dipoles to relax back to their energetically favored random orientations.[30] The intensity of this peak can be decreased or increased based on the poling voltage because a higher voltage results in a more complete alignment of the random dipoles.

The P_2 peak corresponds to the release of subsurface interfacial charge from the material. The C_{60} composite shows a sharp, intense P_2 peak from 0 to 40 °C that is nearly 50 times greater than that of pure PVDF. C_{60}, the more symmetric of the two nanoparticles, allows for a homogeneous nanocomposite with a vast number of small uniformly dispersed charges. The result is a large amount of interfacial charge at low activation energies that can be readily released through charge hopping.[28] It is due to this abundance of hopping sites, pathways, and subsurface charges contained within the C_{60} composite, that the P_2 is so drastically increased.

The SWNT composite shows a less intense P_2 peak that is still about 6 times greater than PVDF. The length of the nanotubes results in greater overlap between nanoparticles, creating low resistance pathways that allow subsurface interfacial charge to instantaneously dissipate to the material surface during poling. This engenders a lower retention of subsurface charge and smaller P_2 peak. However, due to the inhomogeneous nature of the SWNT matrix, more charge resides at deeper levels because of fewer hopping sites with higher energy barriers.

The temperature of the P_3 peak occurrences roughly correspond to the Curie point of PVDF. This is the temperature at which all polarization in the crystalline regions of the polymer is lost and the charges are released. The C_{60} and SWNT composites show P_3 peaks 18 and 9 times greater than pure PVDF, respectively. A larger release of current at the Curie temperature indicates a more efficient polarization of dipoles during poling. Generally, the internal field strength is assumed to be the same as the external field strength when poling, however, previous experimentation has shown that dipole orientation of PVDF is nonuniform, with a more efficient alignment near the surface and internal space charges in the material.[32] The addition of interfacial charge into the material allows for an increased efficiency in dipole polarization, giving rise to a larger P_3 peak.

Additionally, both C_{60} and SWNTs have demonstrated the production of local (internal) electric field enhancements. It has been reported that under an applied external field, C_{60} creates a local field twice as strong, with SWNTs producing similar enhancements.[33,34] Delocalization of electrons in the molecules allows for a strong macroscopic dipole development during poling. Unlike space charge, however, the electrons are present through delocalization in the nanoparticle, thus eliminating the need for charge injection. Due to the increase in electric field offered by these molecules, the effective localized poling radius is greatly increased, leading to a much more uniformly and completely polarized material as schematically represented in Figure 5. In addition, recent reports have suggested that the introduction of heterointerfaces into a material can create localized stress points, increasing domain mobility and facilitating polarization.[35,36]

The final peak, P_4, beginning around 150 °C, corresponds to the flow temperature of the polymer. At this point, all of the low activation energy charges have been released, leaving only deep interfacial charges. Upon melting, the remaining high activation energy charges are liberated from the material. Due to natural inhomogeneity, the SWNT composite contains a large amount of charge trapped at deep levels which is released upon melting, while the C_{60} composite has less charge remaining. Thus, the P_4 SWNT and C_{60} peaks are 25 and 7 times greater than pure PVDF, respectively.

C. Hysteresis testing

Further insight into the effects of creating internal charge can be gained through the use of hysteresis measurements. Figure 6 shows the measured electrical polarization (P) of the samples versus applied electrical field (E), referred to as a PE hysteresis curve. PE curves are essential for validating a material's ferroelectric behavior at a particular temperature and frequency. The dissipation of energy produces a phase separation between the charge and voltage signals giving a loop with a definable area under the curve.[37] This area is an indication of the charge storage capability of the material. For example, a good ferroelectric material will exhibit a large square curve quantified by remnant polarization

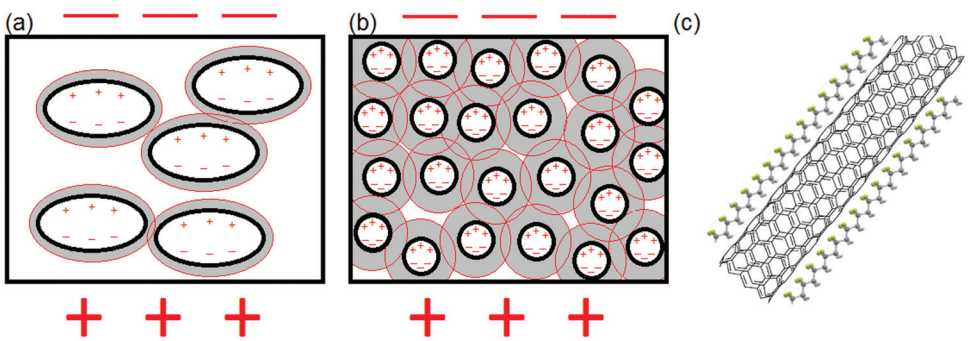

FIG. 5. (a) A typical electret material with large, heterogeneous space charge affecting a small area opposed to (b) a homogenous electretic system with extended poling fields, created by C_{60} in the material. It is worth noting that in reality, the charge develops on the outer edge of the C_{60} structure opposed to the inner free space, and (c) a carbon nanotube with aligned surrounding PVDF due to field enhancement.

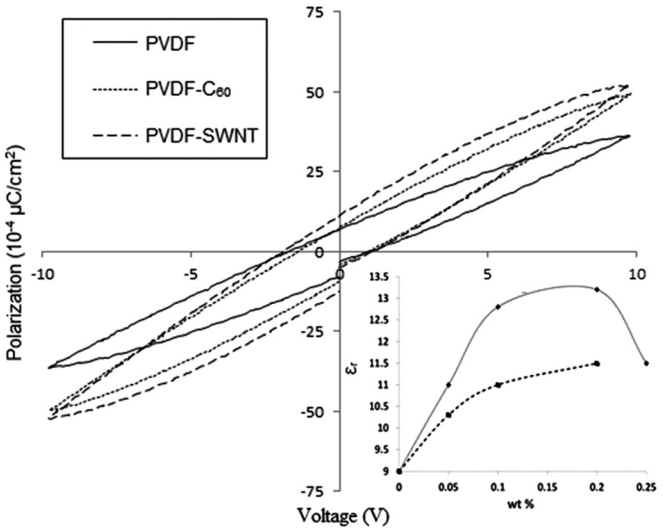

FIG. 6. PE Hysteresis loop of pure PVDF, PVDF-C_{60} (0.1 wt. %), PVDF-SWNT (0.1 wt. %). Inset relative dielectric constant (ε_r) profiles as a function of wt. %.

and coercive field, while a narrow hysteresis loop would indicate a lossy capacitor with a high tanδ (dissipation factor).[38] The linear portion of the curve is proportional to the relative dielectric constant. In an ideal, voidless, ferroelectric polymer, we would expect that charge accumulation is due to the polarization of molecular dipoles. However, in a dielectric composite material, interfacial polarization (Maxwell-Wagner-Sillers polarization) develops due to a swell of charge at the inner dielectric boundaries of the conductively heterogeneous material.[39,40] In this case, the nanoparticles are more conductive than the polymer, resulting in mobilization of charge along the particle perimeters, facilitating hetero-polarization in the material.[41,42] Research exploiting the relationship between interfacial polarization and dielectric characteristics of PVDF-CNT composites has been reported. However, these materials have largely shown lower piezoelectricity than commercial PVDF.[43,44]

Figure 6 shows a PE loop at a voltage of ± 10 V for the PVDF nanocomposites. Testing was conducted at a lower field strength than required to polarize molecular dipoles, thus the observed open curve can only be caused by internal heterogeneous charge. Pure PVDF shows a small amount of internal charge due to voids and impurities, but a significant increase in area and slope for both of the nanocomposites is measured. The shape and field sensitivity of these curves looks much like an electretic material curve. The area under this curve increases with loading percentage as expected from past results, but is naturally limited by conductivity at high loading levels.[4] The increase in the magnitude of remnant polarization is indicative of the fact that molecular dipoles are able to partially align with the applied electric field. We also noticed a shift toward the left axis for the hysteresis loops which is typically indicative of the internal bias field formed due to presence of defect dipoles. In our case, the bias field can be traced to the net ordering of the interfacial charges as discussed in Fig. 5.

The instantaneous slope of the hysteresis curve yields the material's permittivity ($\varepsilon_0\varepsilon_r$), where ε_r is the relative permittivity and ε_0 is the vacuum permittivity (8.85 pF/m).

The inset in Figure 6 is the ε_r profile of the composites as a function of loading level. As the amount of SWNTs is increased there is an increase in ε_r to 11.5 at 0.2 wt. %. The SWNT samples are conductive above this level. The C_{60} composites show a larger increase in ε_r to a maximum of 13.2. A slow decrease in ε_r is observed in the C_{60} composites after the maximum as opposed to the sharp deterioration in the SWNT samples. The spherical shape of C_{60} allows for a higher loading level to be achieved without conduction through the samples because there is a lower overlap between nanoparticles at a given loading level. As the loading level of C_{60} increases the charge sites become nearer to each other, encouraging the dissipation of charge through hopping and thus reducing the overall dielectric constant. Significant overlap between nanotubes upon increase in loading level occurs before a reduction in ε_r, leading to conductivity. Four-point probe conductivity measurements revealed that at a loading level of 0.1%, the SWNT composite was 300% more conductive than the C_{60} composite, however, the difference jumped to 1000× at 0.25 wt. %.

D. Mechanical characteristics

Figure 7 shows the relationship between nanoparticle weight percentage and Young's modulus (Y). Values are lower than previously reported for PVDF, however, they are consistent and reasonable when considering production method and changes in molecular weight can have a significant impact on mechanical properties.[45] Pure PVDF exhibits a modulus of 1.2 GPa and, upon the addition of 0.05 wt. % SWNT, the modulus increases to over 1.3 GPa with a maximum of 1.35 GPa at 0.1 wt. %. The increase in Young's modulus from the addition of SWNTs is limited by entanglements and inhomogeneities. The C_{60} composites have a lower increase in modulus with loading level but a higher maximum value in excess of 1.55 GPa.

Commercially produced, poled and stretched PVDF was tested as a control showing a d_{31} of 31.5 pC/N, which is consistent with the value reported in literature for uniaxially stretched PVDF.[12,46]

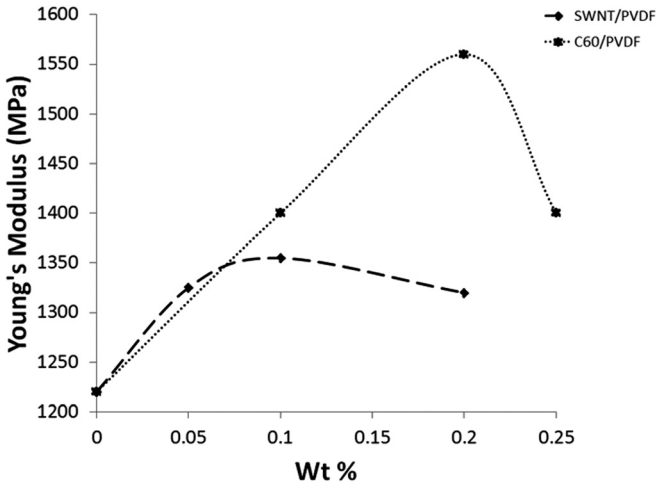

FIG. 7. Young's modulus of PVDF-C_{60} and PVDF-SWNT as a function of nanoparticle wt. % mechanical characteristics.

TABLE I. Piezoelectric d_{31} (pC/N) values for composites.

Wt. %	0	0.1	0.05	0.1	0.2	0.25
C_{60}	32	33	36	44	63	59
SWNT	32	44	65	62	54	NA

As shown in Table I, the SWNT composites reach a maximum d_{31} of 65 pC/N at a loading level of 0.05 wt. %, before declining. The C_{60} composite shows a comparable increase with a maximum d_{31} value of 63 pC/N before declining. Pure PVDF samples made in the same manner as the composites show a d_{31} of 32 pC/N; thus, the composites possess a d_{31} double that of pure PVDF.

While the d_{31} coefficient provides some insight into the charge generated per unit applied force, the electromechanical coupling factor, k, is a measure of the efficiency of energy conversion, and can be expressed as:[47]

$$k_{31} = \frac{d_{31}}{\sqrt{\varepsilon_o \varepsilon_r s_{11}}}, \quad (2)$$

where k_{31} is the coupling coefficient, ε_o is the permittivity of free space, ε_r is the relative dielectric constant, and $s_{11}{}^E$ is the compliance (inverse Y).[48] This relationship is somewhat intuitive in that one would expect a stiffer material to experience larger strains, resulting in larger internal mechanical energy. Also, while increasing the dielectric constant allows for a greater amount of charge generation, it also increases the force needed to move charge, resulting in a lower efficiency. In Eq. (2), if one assumes a constant d_{31}, the k_{31} is proportional to the square of the Y and inversely proportional to ε_r. Thus, one then would expect that by increasing the Y and decreasing ε_r, a very electromechanically efficient material can be realized. However, it is impossible to change only one variable. For example, as Y is increased through the addition of the nanoparticles, ε_r generally increases due to the creation of dielectric boundaries. This results in a performance tradeoff. According to literature, pure PVDF has a k_{31} value of 0.12, and when calculated using the values measured here a k_{31} of 0.125 is obtained.[49] The maximum k_{31} for the C_{60} composites occurs at a loading level of 0.2 wt. % with a value of 0.23; 1.84 times that of pure PVDF. The maximum for the SWNT occurs at a loading level of 0.05 wt. % with a value of 0.25, a value 2 times that of pure PVDF.

IV. CONCLUSIONS

It has been demonstrated that through the addition of SWNTs and C_{60} to PVDF at concentrations less than 0.25 wt. %, the piezoelectric coefficient d_{31} can be enhanced to double that of pure PVDF. This is achieved through a multi-mechanistic enhancement involving the seeding of crystalline sites, creation of internal charge, increased polarization, and the optimization of Young's modulus and dielectric constant. The calculated electromechanical coupling coefficients (k_{31}) at optimal loading levels are 1.84 and 2 times greater than pure PVDF for the PVDF-C_{60} and PVDF-SWNT composites. While both composites experience similar enhancement, the optimum SWNT composite performance occurs at a lower loading level than the C_{60} composites, resulting in a greater retention of the naturally low mechanical compliance and dielectric constant of PVDF. Alternatively, the C_{60} composites offer a more charged, stiff material at higher loading levels. These performance differences allow for a new application specific material. Such novel piezoelectric carbon nanocomposites could be of great value for future applications ranging for broadband sensing to vibration-specific energy-scavenging.

ACKNOWLEDGMENTS

Tetramer Technologies acknowledges support from the National Science Foundation SBRIR Phase II Award (Grant No. 0923988). We also thank the NSF I/UCRC Center for Energy Harvesting Materials & Systems (Grant No. 37155043), the Robert A. Welch Foundation (Grant AT-0041) and the National Science Foundation MWN-GOALI program.

[1]B. Jaffe, W. R. Cook, Jr., and H. Jaffe, *Piezoelectric Ceramics (Nonmetallic Solids, No. 3)* (Academic, 1971), p. 318; Dirk M. Guldi, G. M. Aminur Rahman, V. Sgobba, and Christian Ehli, Chem. Soc. Rev. **35**, 471 (2006).
[2]W. G. Cady, *Piezoelectricity: An Introduction to the Theory and Applications of Electromechanical Phenomena in Crystals*, Revised ed. (Dover, 1964), p. 822.
[3]A. Ballato, IEEE Trans. Ultrason. Ferroelectr. Freq. Control **42**(5), 916 (1995).
[4]J. Kim, K. J. Loh, and J. P. Lynch, Proc. SPIE **6932**, 693232 (2008).
[5]S. R. Anton and H. A. Sodano, Smart Mater. Struct. **16**, R1 (2007).
[6]Y. Yu, X. N. Zhang, and S. L. Xie, Smart Mater. Struct. **18**, 095006 (2009).
[7]B. A. Auld, *Aoustic Fields and Waves in Solids* (Krieger Publishing Company, Melbourne, 1990).
[8]A. Ramaratnam and N. Jalili, J. Intell. Mater. Syst. Struct. **17**, 199 (2006).
[9]H. Kawai, Jpn. J. Appl. Phys. **8**, 975 (1969).
[10]R. Hasegawa, Y. Takahashi, Y. Chatani, and H. Tadokoro, Polym. J. **3**, 600 (1972).
[11]T. Mirfakhrai, J. D. W. Madden, and R. H. Baughman, Mater. Today **10**, 30 (2007).
[12]W. Kunstler, M. Wegener, M. Seiss, and R. Gerhard-Multhaupt, Appl. Phys. A: Mater. Sci. Process. **73**, 641 (2001).
[13]B. A. Newman, P. Chen, K. D. Pae, and J. I. Scheinbeim, J. Appl. Phys. **51**, 5161 (1980).
[14]E. Fukada, Key Eng. Mater. **92–93**, 143 (1994).
[15]S. Zhang, N. Zhang, C. Huang, K. Ren, and Q. Zhang, Adv. Mater. (Weinheim, Ger.) **17**, 1897 (2005).
[16]N. Levi, R. Czerw, S. Xing, P. Iyer, and D. L. Carroll, Nano Lett. **4**, 1267 (2004).
[17]R. E. Newnham, D. P. Skinner, and L. E. Cross, Mater. Res. Bull. **13**, 525 (1978); B. Ploss, B. Ploss, F. G. Shin, H. L. W. Chan, and C. L. Choy, IEEE Trans. Dielectr. Electr. Insul. **7**, 517 (2000).
[18]C. Cui, R. H. Baughman, Z. Iqbal, T. R. Kazmar, and D. K. Dahlstrom, Synth. Met. **85**, 1391 (1997).
[19]E. Venkatragavaraj, B. Satish, P. R. Vinod, and M. S. Vijaya, J. Phys. D: Appl. Phys. **34**, 487 (2001).
[20]T. V. Sreekumar, T. Liu, B. G. Min, H. Guo, S. Kumar, R. H. Hauge, and R. E. Smalley, Adv. Mater. (Weinheim, Ger.) **16**, 58 (2004).
[21]L. Wang and Z.-M. Dang, Appl. Phys. Lett. **87**, 042903 (2005).
[22]A. Salehi-Khojin, M. R. Hosseini, and N. Jalili, Compos. Sci. Technol. **69**, 545 (2009).
[23]H. W. Kroto, J. R. Heath, S. C. O'Brien, R. F. Curl, and R. E. Smalley, Nature (London) **318**, 162 (1985).
[24]E. J. Sharp and L. E. Garn, J. Appl. Phys. **53**, 8980 (1982).
[25]M. Ullah, A. K. Kadashchuk, P. Stadler, A. Kharchenko, A. Pivrikas, C. Simbrunner, N. S. Sariciftci, and H. Sitter, Mater. Res. Soc. Symp. Proc. **1270**, 1270-II06-68 (2010).

[26]S. Bauer, S. Bauer-Gogonea, M. Dansachmuller, I. Graz, H. Leonhartsberger, H. Salhofer, and R. Schwoediauer, Proc.-IEEE Ultrason. Symp. **1**, 370 (2003).
[27]P. Fischer and P. Roehl, Prog. Colloid Polym. Sci. **62**, 149 (1977).
[28]D. K. Das-Gupta, K. Doughty, and R. S. Brockley, J. Phys. D **13**, 2101 (1980).
[29]M. F. Galikhanov, D. A. Eremeev, and R. Ya Deberdeev, Russ. J. Appl. Chem. **76**, 1651 (2003).
[30]M. Abkowitz and G. Pfister, J. Appl. Phys. **46**, 2559 (1975).
[31]T. Mizutani, T. Yamada, and M. Ieda, J. Phys. D **14**, 1139 (1981).
[32]G. M. Sessler, J. Acoust. Soc. Am. **70**, 1596 (1981).
[33]M. Ya Amusia and A. S. Baltenkov, Los Alamos Natl. Lab., arXiv:physics/0604104 (2006).
[34]J. M. Bonard, H. Kind, T. Stockli, and L. O. Nilsson, Solid-State Electron. **45**, 893 (2001).
[35]P. Gao, C. T. Nelson, J. R. Jokisaari, S.-H. Baek, C. W. Bark, Y. Zhang, E. Wang, D. G. Schlom, C.-B. Eom, and X. Pan, Nat. Commun. **2**, 1600/1 (2011).
[36]C. T. Nelson, B. Winchester, Y. Zhang, S.-J. Kim, A. Melville, C. Adamo, C. M. Folkman, S.-H. Baek, C.-B. Eom, D. G. Schlom, L.-Q. Chen, and X. Pan, Nano Lett. **11**, 828 (2011).
[37]M. W. Barsoum, *Fundamentals of Ceramics* (IOP Publishing, 2003), p. 603.
[38]M. G. Cain, M. Stewart, M. G. Gee, G. J. Hill, and D. Hall, Report No. 1361-4061, 1998.
[39]E. Godzhaev, A. Magerramov, S. Osmanova, M. Nuriev, and E. Allakhyarov, Surf. Eng. Appl. Electrochem. **43**(2), 148 (2007).
[40]R. W. Sillars, J. Inst. Electr. Eng. **80**(484), 378 (1937).
[41]Z. Ounaies, C. Park, K. E. Wise, E. J. Siochi, and J. S. Harrison, Compos. Sci. Technol. **63**, 1637 (2003).
[42]Z. Ounaies, C. Park, J. S. Harrison, N. M. Holloway, and G. K. Draughon, U.S. patent 7402264B2 March 3 (2008).
[43]Z.-M. Dang, S.-H. Yao, and H.-P. Xu, Appl. Phys. Lett. **90**, 012907 (2007).
[44]A. Salehi-Khojin and N. Jalili, Composites, Part B **39**, 986 (2008).
[45]Q. Chen, D. Natale, B. Neese, K. Ren, M. Lin, Q. M. Zhang, M. Pattom, K. W. Wang, H. Fang, and E. Im, Proc. SPIE **6524**, 65241P (2007).
[46]E. Fukada, IEEE Trans. Ultrason. Ferroelectr. Freq. Control **47**, 1277 (2000).
[47]A. H. Meitzler, H. F. Tiersten, A. W. Warner, D. Berlincourt, G. A. Coquin, and F. S. Welsh, III, *IEEE Standard on Piezoelectricity* (IEEE, New York, 1978).
[48]M. Schwartz, *Smart Materials* (CRC, 2009).
[49]"*Piezoelectric Polymers,*" Encyclopedia of Smart Materials A, edited by J. S. Harrison and Z. Ounaies Biderman (John Wiley & Sons, 2002), p. 162.